Adaptive Spatial Registration for Electromagnetic Surgical Navigation Via Deep Learning

Gaoshuai Chen. Yi Gan. Xinyao Li.

College of Mechanical Engineering, University of Shanghai for Science and Technology, China

Abstract: *Electromagnetic navigation systems are essential for precise instrument positioning during radiofrequency ablation procedures, yet their accuracy is often compromised by electromagnetic field distortions from surgical equipment and environmental interference. This study presents a novel deep learning-based spatial registration framework incorporating self-attention mechanisms for adaptive weighting of global and local spatial features. We introduce a dynamic weighted loss function that progressively optimizes the model from global feature learning to precise local registration. Experimental results demonstrate superior performance, with 80% of registration points achieving Euclidean distance errors below 0.8 units and a Local Feature Preservation Rate of 96.08%. The framework maintains robust accuracy under varying electromagnetic conditions, achieving an overall Root Mean Square Error of 0.6075 and End-to-end Point Mapping Accuracy of 92.74%. Bland-Altman analysis confirms minimal systematic bias, with 95% of measurements within ±1.96 standard deviations. This research advances computer-assisted surgical navigation by providing a robust solution for precise instrument tracking in challenging electromagnetic environments, thereby improving the safety and efficacy of radiofrequency ablation procedures.*

Keywords: *Attention Mechanism, Deep Learning, Electromagnetic Navigation, Feature Fusion, Radiofrequency Ablation, Spatial Registration*

I. Introduction

Recent advances in precision medicine have revolutionized minimally invasive therapeutic approaches, with radiofrequency ablation (RFA) emerging as a pivotal intervention in oncological treatment[1]. RFA operates through the generation of localized hyperthermia to induce tumor cell death, with its therapeutic efficacy and safety profile fundamentally dependent on precise ablation zone control[2]. Despite significant technological progress, the complex anatomical architecture of human tissue and the dynamic nature of intraoperative changes present substantial challenges. While conventional image-guided techniques provide valuable preoperative planning data, they are inherently limited in their capacity to offer real-time instrument tracking and navigation capabilities. This limitation

significantly impacts procedural precision and safety parameters, making accurate instrument positioning and continuous monitoring a critical unmet need in clinical practice[3, 4]. Electromagnetic navigation systems have garnered considerable attention in surgical navigation due to their distinctive advantages, including real-time tracking capability, radiation-free operation, and immunity to line-of-sight restrictions. These systems represent a promising solution to address the current limitations in precise surgical navigation.

Electromagnetic navigation systems fundamentally rely on electromagnetic tracking technology, which establishes spatial correspondence between the electromagnetic field coordinate system and medical imaging coordinate system through strategically positioned electromagnetic sensors on the patient's surface[5]. However, the clinical implementation of electromagnetic navigation systems faces significant technical challenges. The primary concern stems from the susceptibility of electromagnetic fields to external interference, resulting in non-linear distortions in measurement data[6]. Conventional registration methodologies demonstrate limited efficacy in addressing these non-linear deformations, particularly in localized regions where registration accuracy frequently fails to meet clinical requirements. Furthermore, the presence of metallic equipment and electronic instruments in the surgical environment exacerbates electromagnetic field inhomogeneity, substantially increasing the complexity of spatial registration[7, 8]. Such precision degradation may lead to critical misjudgments in the spatial relationships between surgical instruments and vital anatomical structures, thereby elevating procedural risks[9].

To address these challenges, we propose a novel adaptive spatial registration method based on deep learning architecture. This approach transcends the limitations of conventional rigid registration while avoiding the pitfalls of non-rigid registration methods that prioritize global alignment at the expense of point-specific accuracy. Our method achieves precise spatial mapping of individual registration points in complex electromagnetic environments through an innovative deep learning architecture that integrates global and local transformation features. We introduce a self-attention mechanism that enables adaptive weighting of global and local features, significantly enhancing registration accuracy and robustness. Additionally, we implement a dynamic loss function training strategy that facilitates progressive optimization from global feature learning to local precise registration, effectively balancing registration accuracy across different regions.

The primary contributions of this study are threefold:

1. Development of an innovative electromagnetic navigation spatial registration framework capable of effectively addressing non-linear deformation in electromagnetic field environments.
2. Design of a feature fusion strategy based on self-attention mechanisms, enabling adaptive modeling of complex spatial transformations.
3. Introduction of a dynamic weighted loss function that optimizes the model training process, enhancing overall system performance and stability.

II. Research Status

Significant advances have been achieved in electromagnetic navigation-assisted surgery in recent years. Boveiri et al.[10]conducted a comprehensive review of deep learning applications in multimodal medical image registration,

highlighting current research directions and challenges. In a prospective cohort study focusing on radiofrequency ablation of liver tumors, Ringe et al.[11]demonstrated the clinical feasibility of electromagnetic navigation guidance. Gao et al. [12]performed a systematic comparison between optical and electromagnetic tracking systems in image-guided interventional procedures. Franz et al.[13]proposed a standardized evaluation methodology for novel compact field generators, providing crucial insights for improving system performance in complex environments.

In the domain of deep learning methodologies, Yu et al.[14]pioneered an end-to-end learning approach integrating deep learning with electromagnetic navigation systems, effectively addressing non-linear deformation challenges in medical applications. Wang et al.[15]further advanced the field by introducing a pyramid attention network for medical image registration, achieving substantial improvements in registration stability and accuracy. These contributions have provided innovative solutions for addressing electromagnetic field inhomogeneity issues.

Regarding multimodal fusion strategies, Wei et al.[16]developed a progressive learning approach based on gradient attention mechanisms, enabling dynamic optimization of registration accuracy. Haskins et al.[17]provided a comprehensive survey of deep learning applications in medical image registration, synthesizing key challenges in current research. Miao et al.[18]implemented real-time 2D/3D registration through CNN regression, offering an efficient solution for enhancing system real-time performance.

III. Methods

We propose an electromagnetic navigation system for radiofrequency ablation procedures, incorporating neural networks to enhance three-dimensional positioning accuracy of surgical instruments. The system employs a multi-stage framework to address the inherent challenges of electromagnetic tracking in surgical environments. Initially, electromagnetic sensors are strategically positioned on the patient's surface as registration fiducials, establishing spatial correspondence between the electromagnetic field coordinate system and medical imaging coordinate system. The system integrates electromagnetic sensors at the surgical instrument tip, combining geometric parameters with end-effector pose information to achieve real-time tracking capability.

3.1 Spatial Registration Framework

Spatial registration represents a critical process for precise alignment of data between different coordinate systems. In radiofrequency ablation procedures, traditional methods face significant limitations in real-time monitoring of spatial relationships between ablation needles and critical anatomical structures due to the inherent invisibility of surgical instruments within the human body. Moreover, these methods struggle to accurately assess the relative position between the needle tip and target lesions. Let $P = \{p_i\}_{i=1}^{n}$ denote the point set in the electromagnetic field coordinate system and $Q = \{q_i\}_{i=1}^{n}$ represent the corresponding point set in the medical imaging coordinate system. Our objective is to establish the mapping function $f : P \to Q$ to enable real-time visualization of surgical instrument positioning within medical images. Considering the complexity of the electromagnetic field environment and uncertainty factors in the registration process, we propose a deep

learning-based registration method to enhance system accuracy and robustness.

3.2 Deep Neural Network Architecture for Spatial Registration

This study formulates the registration problem as a spatial mapping from electromagnetic field source point sets to medical image target point sets. In the ideal scenario, the spatial transformation can be expressed as:

$$q_i = Rp_i + t + ò \tag{1}$$

where R represents the rotation matrix, t denotes the translation vector, and ò indicates random noise. However, considering the non-uniform electromagnetic field distribution caused by environmental interference in surgical settings, the actual transformation incorporates nonlinear components:

$$q_i = f(p_i) = f_{global}(p_i) + f_{local}(p_i) \tag{2}$$

where f_{global} represents the global affine transformation and f_{local} denotes the local non-rigid transformation. To effectively handle such complex spatial transformations, we propose a novel deep learning architecture that integrates both global and local transformation components.

As illustrated in Fig.1, our network architecture comprises the following key modules:

1. Feature Extraction Module: We employ one-dimensional convolutional neural networks (1D CNN) to extract features from both source and target point sets. Compared to traditional multilayer perceptrons (MLPs), convolutional operations demonstrate superior capability in capturing local spatial structures and geometric features while preserving topological relationships within point cloud data.
2. Feature Enhancement Module: We implement max-pooling operations to extract salient features, followed by L2 normalization to generate feature vectors for both source and target point sets. Subsequently, we construct a similarity matrix using these normalized features. The cosine similarity metric is adopted as the loss function, offering robust performance against scale variations.
3. Spatial Information Fusion Module: For each point requiring registration, we employ a dual-layer 1D CNN architecture, followed by global max-pooling and L2 normalization for spatial feature extraction. The extracted features are then deeply integrated with source point set feature vectors through a self-attention mechanism.
4. Coordinate Prediction Module: The fused features undergo dimensionality reduction through two fully connected layers, ultimately generating three-dimensional spatial coordinates (x, y, z) to complete the point mapping.

This hierarchical architecture effectively captures the complexity of spatial transformations through multi-level feature extraction and fusion. The incorporation of the self-attention mechanism enables adaptive weighting of local and global features, thereby enhancing registration accuracy. Moreover, our approach demonstrates robust performance in handling both rigid and non-rigid transformations, making it particularly suitable for surgical navigation applications where electromagnetic field distributions may be irregular.

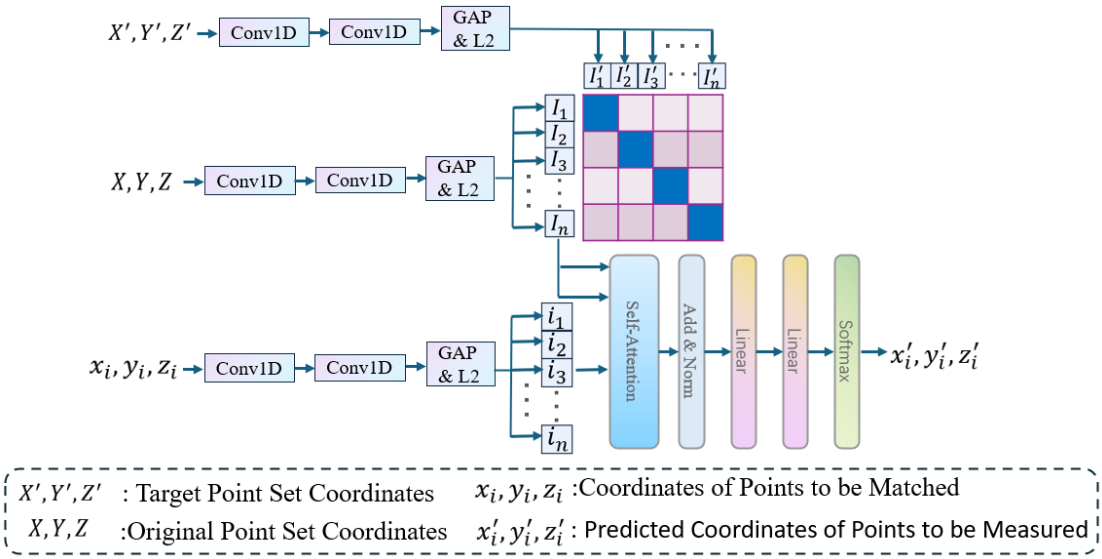

Figure 1. Framework Diagram of the Neural Network Algorithm

3.3 Attention-based Feature Fusion Module

The feature fusion module serves as a critical component in achieving high-precision spatial registration, with its primary objective being the effective integration of local features from individual registration points with global features from the source point set. In the context of radiofrequency ablation surgical navigation, exclusive reliance on local features may result in registration outcomes being overly sensitive to local electromagnetic field disturbances, while sole consideration of global features risks overlooking crucial local geometric properties within the surgical region. To address these challenges, we propose an attention-based feature fusion strategy that adaptively balances local and global information, thereby enhancing both registration accuracy and robustness.

As illustrated in Fig.2, our feature fusion process encompasses three primary stages: feature mapping matrix generation, attention weight computation, and feature aggregation. During the feature mapping stage, let $h_i \in \mathrm{R}^d$ represent the feature vector of a single registration point and $H = \{h_1, h_2, ..., h_n\} \in \mathrm{R}^{n \times d}$ denote the feature matrix of the source point set, where represents the source point set size and d indicates the feature dimension. Considering that each registration point must engage in attention computation with all points in the source set while accounting for their collective influence, we generate Query (Q), Key (K), and Value (V) matrices through linear transformations:

$$\begin{cases} Q = h_i W_q \in \mathrm{R}^{1 \times d} \\ K = H W_k \in \mathrm{R}^{n \times d} \\ V = H W_v \in \mathrm{R}^{n \times d} \end{cases} \tag{3}$$

Where $W_q, W_k, W_v \in \mathrm{R}^{d \times d}$ represent learnable weight matrices. This architectural design enables the Query matrix to capture registration point features, the Key matrix to characterize discriminative features from the source point set, and the Value matrix to encode comprehensive feature information.

In the attention weight computation phase, we calculate the correlation between the registration point and each point in the source set

through dot-product operations between Query and Key matrices. The resulting correlations are transformed into probability distributions via the Softmax function to obtain attention weights:

$$W = \text{softmax}(S) = \text{softmax}\left(\frac{QK^T}{\sqrt{d}}\right) \tag{4}$$

where $\sqrt{d}$ acts as a scaling factor to regulate gradient magnitudes. The application of the Softmax function ensures non-negativity and normalization of attention weights, enabling the network to adaptively allocate importance across different spatial positions.

The final fused features are obtained through weighted summation:

$$F_{fused} = W \times V \tag{5}$$

The fused features F_{fused} preserve both the local geometric characteristics of the registration point and the spatial information from the source point set. Our proposed feature fusion mechanism demonstrates several technical advantages in spatial registration tasks: The attention mechanism enables adaptive weight distribution, allowing the model to dynamically adjust feature fusion weights based on spatial correlations, thereby enhancing system adaptability to varying degrees of electromagnetic field disturbances. The incorporation of global spatial information from the source point set within the fused features enhances registration generalization performance, enabling the system to handle complex spatial transformations encountered in surgical navigation. The integration of the attention mechanism enables the model to capture complex nonlinear spatial relationships, providing robust support for handling local deformations in surgical environments.

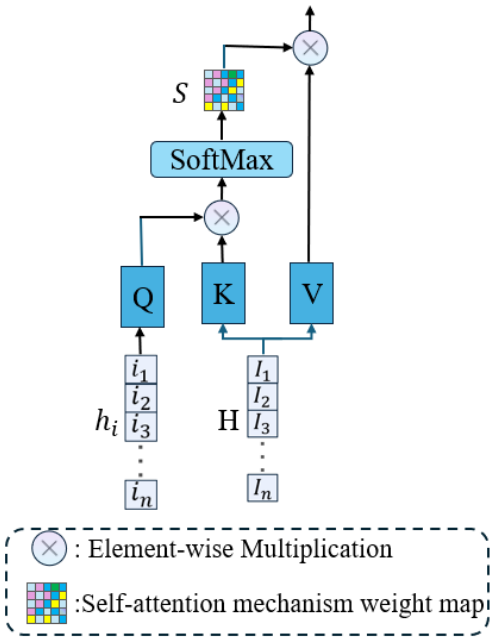

Figure 2. Framework Diagram of the Feature Fusion Algorithm

3.4 Multi-objective Loss Function with Dynamic Weighting

To optimize the spatial registration network, we propose a composite loss function that integrates contrastive learning loss with point position error loss, incorporating a dynamic weight adjustment mechanism. The design of the loss function aims to achieve progressive optimization from global feature learning to precise local registration.

For training samples with batch size N, let H_s *and* H_t denote the feature matrices of source and target point sets, respectively. The contrastive loss is formulated as:

$$L_{contrast} = -\frac{1}{N}\sum_{i=1}^{N}\log\frac{\exp(sim(H_{s,i}, H_{t,i})/\tau)}{\sum_{j=1}^{N}\exp(sim(H_{s,i}, H_{t,j})/\tau)} \tag{6}$$

where τ is a temperature parameter controlling the smoothness of feature distribution, and $sim(h_{s,i}, h_{t,j})$ represents the cosine similarity between the i-th source feature and the j-th target feature:

$$sim(h_{s,i}, h_{t,j}) = \frac{H_{s,i}^T H_{t,j}}{\| H_{s,i} \| \cdot \| H_{t,j} \|} \tag{7}$$

For individual point predictions, we employ Euclidean distance loss to measure the error between predicted and ground truth coordinates:

$$L_{pos} = \frac{1}{N} \sum_{i=1}^{N} \| q_i - \hat{q}_i \|_2^2 \tag{8}$$

where $q_i = (x_i, y_i, z_i)$ and $\hat{q}_i = (\hat{x}_i, \hat{y}_i, \hat{z}_i)$ represent the ground truth and predicted coordinates, respectively. In this study, we have implemented a Dynamic Weight Adjustment Strategy, wherein the total loss function is augmented with adaptive weights:

$$L_{total} = \lambda_1(t) L_{contrast} + \lambda_2(t) L_{pos} \tag{9}$$

To achieve smooth transition from global feature learning to local precise registration, we design a training progress-based dynamic weight adjustment strategy:

$$\begin{cases} \lambda_1(t) = \lambda_{1,max} \cdot \exp(-\alpha t / T) \\ \lambda_2(t) = \lambda_{2,min} + (\lambda_{2,max} - \lambda_{2,min})(1 - \exp(-\beta t / T)) \end{cases} \tag{10}$$

wheret denotes the current training step，T represents the total number of training steps，$\lambda_{1,max}$ is the initial maximum weight for contrastive learning loss，$\lambda_{2,min}$ and $\lambda_{2,max}$ are the minimum and maximum weights for position error loss, αandβare hyperparameters controlling weight transition rates.

IV. Experimental

4.1 Data Enhancement and Processing

The initial experimental setup comprised six sensor-based landmarks, yielding six corresponding coordinate points. However, this limited dataset was insufficient for robust neural network training. Therefore, we developed a comprehensive data augmentation approach to expand the dataset while preserving spatial relationships and geometric properties. The data enhancement process began with a systematic generation of triangular surfaces by implementing a combinatorial approach, selecting three points from the six landmarks (C(6,3)), resulting in 20 unique triangular surfaces. Each surface was defined by its three vertex points, establishing the fundamental geometric elements for subsequent processing. For each triangular surface, we employed a uniform grid sampling method to generate intermediary points through linear combination of the vertex coordinates in the source plane. The transformation between source and target planes was accomplished using Thin Plate Spline (TPS) interpolation, which provides a robust framework for smooth, non-rigid mapping. The TPS transformation was implemented using Radial Basis Functions (RBF), where the RBF kernel computed distance-based relationships between input points and control points. Interpolation weights were derived from the spatial relationships between source points and control points, and a smooth interpolation function was constructed using the RBF framework to determine the precise mapping of grid points from source to target planes.

The final dataset was assembled by systematically collecting corresponding point pairs from both source and target planes, incorporating the original landmark positions, generated grid points and their mapped coordinates, while ensuring geometric consistency through verified point correspondences. This augmentation process significantly expanded the training dataset while maintaining the intrinsic spatial relationships present in the original landmark configuration, thereby providing a more robust foundation for neural network training. The enhanced dataset not only increased the quantity of training samples but also preserved the essential geometric relationships inherent in the original landmark configuration, ensuring that the augmented data maintained physical feasibility while providing sufficient variation to train a robust neural network model. Fig.3 illustrates the spatial relationships between the original coordinate points and the augmented data points across three selected surfaces. In this figure, the original landmark points are denoted by red markers, while the blue and green markers correspond to the newly generated data points through the data augmentation process.

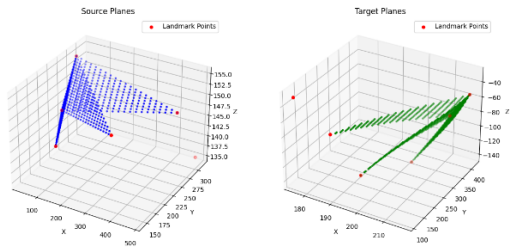

Figure 3. Spatial Relationship Diagram of Original and Augmented Point Sets.

4.2 Implementation Details

In the data preprocessing phase, we performed normalization on the corresponding point data to achieve a unified scale distribution, thereby accelerating neural network convergence and enhancing model performance and generalization capabilities. Within the neural network architecture, L2 normalization was applied to the feature vectors of both source and target point sets prior to similarity matrix computation. This operation scaled high-dimensional vectors to unit norm, effectively mitigating gradient vanishing and explosion issues while maintaining feature consistency.

The neural network implementation was based on the PyTorch framework and conducted on an NVIDIA RTX 2060 GPU. The model was trained with a batch size of 16 using the Adam optimizer with an initial learning rate of 1e-3. We employed CosineAnnealingLR[19] as the learning rate scheduler, allowing for a maximum of 300 training epochs during which the learning rate linearly decayed from its initial value to 1e-5. In the dynamic weight adjustment strategy, we set $\lambda_{1,max} = 0.9$, $\lambda_{2,min} = 0.1$, and $\lambda_{2,max} = 0.9$, with decay/growth rate parameters $\alpha = 2$ and $\beta = 3$, respectively, to ensure smooth transition between global and local feature learning phases.

To quantitatively evaluate the proposed method's performance, we adopted a comprehensive set of complementary evaluation metrics. These metrics were carefully selected to assess algorithm performance across various aspects of point cloud registration and single-point mapping tasks. Specifically, we utilized Root Mean Square Error (RMSE) to evaluate registration accuracy, Chamfer Distance (CD) to measure global similarity between point clouds, Local Feature Preservation Rate (LFPR) to examine local structure preservation performance, and End-to-end Point Mapping Accuracy (EPMA) to assess single-point mapping capability. The mathematical definitions of these metrics are as

follows:

$$\begin{cases} RMSE = \sqrt{\frac{1}{N}\sum_{i=1}^{N} \| p_i^s - p_i^t \|_2^2} \\ CD = \frac{1}{|P_s|}\sum_{x\in P_s} \min_{y\in P_t} \| x-y \|_2 + \frac{1}{|P_t|}\sum_{y\in P_t} \min_{x\in P_s} \| x-y \|_2 \\ LFPR = \frac{1}{N}\sum_{i=1}^{N} \frac{|N_k(p_i^s) \cap N_k(p_i^t)|}{k} \times 100\% \\ EPMA = \frac{1}{M}\sum_{i=1}^{M} 1(\| p_i^{pred} - p_i^{gt} \|_2 < \tau) \end{cases} \quad (11)$$

In these metrics, p_i^s and p_i^t represent the coordinates of corresponding points in the transformed source point cloud and target point cloud, respectively, with N denoting the total number of point pairs. The set $N_k(p)$ represents the k-nearest neighbors of point p, while p_i^{pred} and p_i^{gt} denote the predicted and ground truth point coordinates, respectively. The predefined threshold τ is set to 1.0, and M represents the total number of test points. To ensure evaluation reliability, all metrics were computed on a standardized test set encompassing scenarios with various types and degrees of non-rigid deformations.

4.3 Experimental Results

To comprehensively evaluate the performance of the proposed method, we conducted a multi-dimensional quantitative analysis employing Cumulative Error Distribution (CED) curves, error distribution histograms, three-dimensional error distribution maps, and Bland-Altman analysis, combined with multiple evaluation metrics for systematic assessment of registration results.

The CED curve analysis (Fig4(a)) reveals distinctive distribution characteristics of registration accuracy. The curve exhibits a significant ascending trend within the low error threshold range, indicating high-precision registration for the majority of predicted points. Specifically, approximately 80% of registration points achieved Euclidean distance errors below 0.8 units, and effective registration was accomplished for virtually all points at an error threshold of 1.4. This distribution pattern substantiates the algorithm's robustness and high precision in point cloud registration tasks. The error distribution histogram (Fig4(b)) further quantifies the statistical characteristics of registration accuracy. Results demonstrate that errors predominantly concentrate in the low-value interval below 0.4, corroborating the high-precision characteristics reflected in the CED curve. Notably, the histogram reveals sporadic anomalous values in high-error intervals, prompting a more detailed spatial distribution analysis. The three-dimensional error distribution map (Fig4(c)) unveils the spatial variation pattern of errors: the core region (blue area) exhibits excellent registration accuracy, while peripheral regions show slightly increased errors due to interference sources, resulting in complex nonlinear transformations. This spatial dependency provides crucial insights for further algorithm optimization.

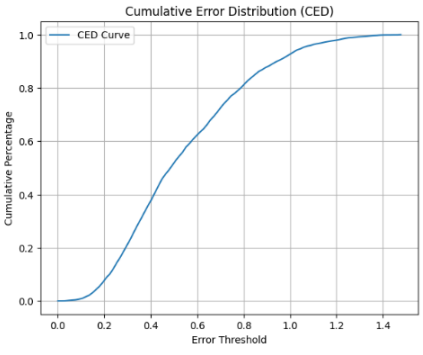

Figure 4(a). CED Curve Chart

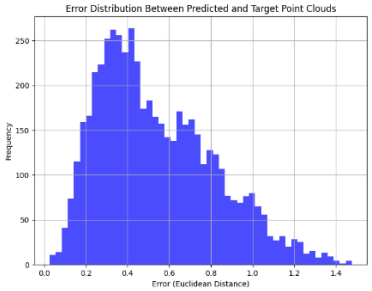

Figure 4(b). Error Distribution Histogram

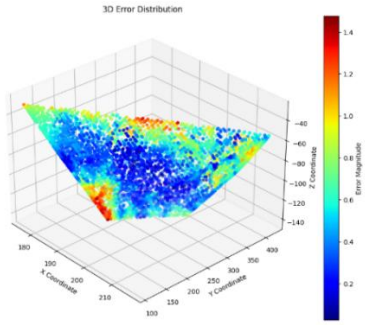

Figure 4(c). Three-Dimensional Error Distribution Plot

To assess systematic bias in registration results, we employed Bland-Altman analysis (Fig.5). Results demonstrate that 95% of data points fall within ±1.96 standard deviations, with mean bias approaching zero, confirming strong agreement between predicted and true values. Notably, relatively apparent error bias was observed along the Y-axis, potentially attributable to interference effects on the magnetic field in this direction. However, the absence of significant trending in errors across spatial coordinates indicates stable predictive performance across different spatial locations.

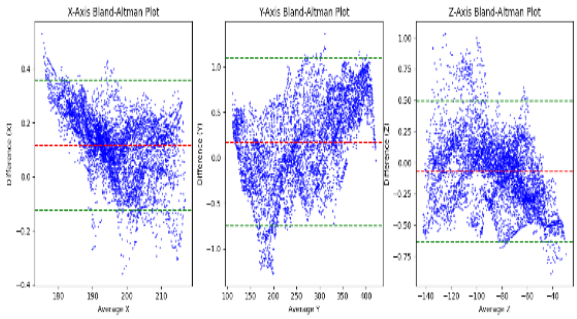

Figure 5. BA Diagram of Predicted Points and Target Points.

Furthermore, we quantitatively evaluated registration performance using standardized metrics, as presented in Table 1:

Table 1. Registration Performance Metrics

RMSE	CD	LFPR	EPMA
0.6075	0.5205	96.08%	92.74%

The RMSE of 0.6075 indicates minimal overall deviation between predicted and target point clouds. The CD of 0.5205 further validates the high geometric similarity between point cloud pairs. Particularly noteworthy is the LFPR of 96.08%, highlighting the algorithm's exceptional performance in preserving local geometric features. Additionally, the EPMA of 92.74% (threshold τ=1.0) confirms high point-matching precision. These metrics collectively constitute a comprehensive evaluation framework, validating the effectiveness and reliability of the proposed method.

V. Conclusion

This study presents a novel deep learning-based spatial registration framework for electromagnetic navigation in radiofrequency ablation procedures, demonstrating significant improvements in registration accuracy and robustness under complex surgical environments. The proposed architecture effectively addresses the challenges of electromagnetic field distortion through several key innovations.

Our attention-based feature fusion mechanism successfully integrates global and local spatial information, enabling adaptive modeling of complex spatial transformations. The quantitative evaluation reveals superior performance, with 80% of registration points achieving Euclidean distance

errors below 0.8 units and an overall Root Mean Square Error (RMSE) of 0.6075. The high Local Feature Preservation Rate (LFPR) of 96.08% particularly demonstrates the method's effectiveness in maintaining crucial geometric relationships, while the End-to-end Point Mapping Accuracy (EPMA) of 92.74% confirms reliable point-specific registration performance.

The implementation of a dynamic weighted loss function strategy has proven instrumental in achieving balanced optimization between global feature learning and local precise registration. Bland-Altman analysis confirms the absence of systematic bias in registration results, with 95% of data points falling within ±1.96 standard deviations. The spatial error distribution analysis reveals consistently high accuracy in core surgical regions, with slightly increased errors in peripheral areas attributable to environmental interference effects.

These results suggest that our proposed method offers a promising solution for enhancing the precision and reliability of electromagnetic navigation in minimally invasive surgical procedures. The framework's ability to maintain high registration accuracy under varying electromagnetic field conditions addresses a critical challenge in clinical applications. Future work should focus on real-time performance optimization and integration with diverse surgical navigation scenarios, potentially extending the methodology to other minimally invasive procedures requiring precise instrument tracking.

The successful development and validation of this registration framework represents a significant step forward in improving the safety and efficacy of radiofrequency ablation procedures through enhanced electromagnetic navigation capabilities. These advancements contribute to the broader field of computer-assisted surgical navigation and demonstrate the potential of deep learning approaches in addressing complex clinical challenges.

References

[1] Takayama, T., et al., Surgery versus Radiofrequency Ablation for Small Hepatocellular Carcinoma: A Randomized Controlled Trial (SURF Trial).*Liver Cancer*, *11*(*3*).2022. 209-218.

[2] Ahmed, M., et al., Image-guided tumor ablation: standardization of terminology and reporting criteria--a 10-year update.*J Vasc Interv Radiol*, *25*(*11*).2014. 1691-705.e4.

[3] Brouwer de Koning, S.G., et al., Electromagnetic surgical navigation in patients undergoing mandibular surgery.*Sci Rep*, *11*(*1*).2021. 4657.

[4] Kim, Y.-s., et al., The Minimal Ablative Margin of Radiofrequency Ablation of Hepatocellular Carcinoma (> 2 and < 5 cm) Needed to Prevent Local Tumor Progression: 3D Quantitative Assessment Using CT Image Fusion.*American Journal of Roentgenology*, *195*(*3*).2010. 758-765.

[5] Ringe, K.I., et al., Electromagnetic Navigation System-Guided Microwave Ablation of Hepatic Tumors: A Matched Cohort Study.*Cardiovasc Intervent Radiol*, *44*(*3*).2021. 500-506.

[6] Teatini, A., et al., The effect of intraoperative imaging on surgical navigation for laparoscopic liver resection surgery.*Sci Rep*, *9*(*1*).2019. 18687.

[7] Franz, A.M., et al., Electromagnetic tracking for US-guided interventions: standardized assessment of a new compact field generator.*Int*

J Comput Assist Radiol Surg, *7*(*6*).2012. 813-8.

[8] Iommi, D., et al., 3D ultrasound guided navigation system with hybrid image fusion.*Sci Rep*, *11*(*1*).2021. 8838.

[9] Denton, W.D., N. Meredith, and M. Ozen, Tracking and Navigation Technologies for Image-Guided Trans-Arterial Interventions.*Techniques in Vascular and Interventional Radiology*.2024. 101010.

[10] Boveiri, H.R., et al., Medical image registration using deep neural networks: A comprehensive review.*Computers & Electrical Engineering*, *87*.2020. 106767.

[11] Ringe, K.I., et al., Electromagnetic Navigation System-Guided Microwave Ablation of Hepatic Tumors: A Matched Cohort Study.*CardioVascular and Interventional Radiology*, *44*(*3*).2021. 500-506.

[12] Xiao, G., et al., Electromagnetic tracking in image-guided laparoscopic surgery: Comparison with optical tracking and feasibility study of a combined laparoscope and laparoscopic ultrasound system.*Med Phys*, *45*(*11*).2018. 5094-5104.

[13] Franz, A.M., et al., Electromagnetic tracking for US-guided interventions: standardized assessment of a new compact field generator.*International Journal of Computer Assisted Radiology and Surgery*, *7*(*6*).2012. 813-818.

[14] Yu, R., et al. *Modeling Electromagnetic Navigation Systems for Medical Applications using Random Forests and Artificial Neural Networks*. in *2020 IEEE International Conference on Robotics and Automation (ICRA)*. 2020.

[15] Wang, Z., H. Wang, and Y. Wang. *Pyramid Attention Network for Medical Image Registration*. in *2024 IEEE International Symposium on Biomedical Imaging (ISBI)*. 2024.

[16] Wei, Z., C. Jung, and C. Su, RegiNet: Gradient guided multispectral image registration using convolutional neural networks.*Neurocomputing*, *415*.2020. 193-200.

[17] Haskins, G., U. Kruger, and P. Yan, Deep learning in medical image registration: a survey.*Machine Vision and Applications*, *31*(*1*).2020. 8.

[18] Miao, S., et al. *Real-time 2D/3D registration via CNN regression*. in *2016 IEEE 13th International Symposium on Biomedical Imaging (ISBI)*. 2016.

[19] Loshchilov, I. and F. Hutter, SGDR: Stochastic Gradient Descent with Warm Restarts.*arXiv: Learning*.2016.